Catalyzed Kinetic Growth in Two-Dimensional MoS_2

Lingli Huang,[a],[b] Quoc Huy Thi,[a],[b] Fangyuan Zheng[c][d], Xin Chen,[a] Yee Wa Chu,[a] Chun-Sing Lee,[a] Jiong Zhao,*[c],[d] Thuc Hue Ly*[a],[b]

[a] Ms. L. Huang, Mr. Q. H. Thi, Mr. X. Chen, Miss Y. W. Chu, Prof. C. S. Lee, Dr T. H. Ly
Department of Chemistry and Center of Super-Diamond & Advanced Films (COSDAF)
City University of Hong Kong
Kowloon, Hong Kong, China
E-mail: thuchly@cityu.edu.hk

[b] Ms. L. Huang, Mr. Q. H. Thi, Dr T. H. Ly
City University of Hong Kong Shenzhen Research Institute
Shenzhen, China
E-mail: thuchly@cityu.edu.hk

[c] Dr. J. Zhao
Department of Applied Physics
The Hong Kong Polytechnic University
Kowloon, Hong Kong, China.
E-mail: jiongzhao@polyu.edu.hk

[d] Dr. J. Zhao
The Hong Kong Polytechnic University Shenzhen Research Institute
Shenzhen, China.
E-mail: jiongzhao@polyu.edu.hk

ABSTRACT: It remains difficult to control the morphology of two-dimensional (2D) materials via direct chemical vapor deposition (CVD) growth. In particular, off-equilibrium (kinetic) growth may produce flakes with non-Wulff shapes (e.g., high-index edges, symmetrical shapes, etc.), which are potentially useful, however a general controllable approach for the kinetic growth of 2D materials are currently lacking. In this work, we pushed the CVD growth of 2D MoS_2 into deep kinetic regime, by using potassium chloride (KCl) as catalyst and plasma pre-treatment on growth substrates. The unprecedented non-equilibrium high-index faceting and unusual high-symmetry shapes in 2D materials have been realized. The growth mechanism of high-index facets is rationalized based on the theory of kinetic instability on crystal surfaces. This new vapor-liquid-adatom-solid (VLAS) growth mechanism—synergistic capture of multiple vapor phase molecules by the catalyst particles on corners and the oversaturated adatom diffusion along adjacent edges can offer great opportunities for shape engineering on 2D materials. The high-quality, rapid and controllable synthesis of high-index facets (edges) and other non-Wulff shapes of 2D transition metal dichalcogenides will benefit the developments in 2D materials.

Explosive research on two-dimensional (2D) transition metal dichalcogenides (TMD) in the past decade have shown their impressive performances in ultrathin and flexible electronics/optoelectronics,[1-5] as well as the rising potentials for emergent valleytronics[5-8] and 2D heterostructures.[9-11] To date, the most controllable growth method for 2D TMDs is chemical vapor deposition (CVD).[12-14] With either homogeneous or heterogeneous nucleation,[15-17] CVD growth under near-equilibrium can often yield high quality single-crystalline 2D TMD flakes,[16,18,19] possibly followed by flake stitching for growing continuous films.[19,20] In-equilibrium crystal shapes or surfaces should follow the Wulff construction,[21,22] minimizing the total surface free energies. The CVD growth of 2D MoS_2 have been predominantly applied in the near equilibrium conditions, hence the shapes of the as-grown single crystal flakes are dominant triangular or occasionally hexagonal.[23,24] The thermodynamic energies of the most stable Mo or S zigzag edges have been explicitly investigated by us,[25,26] as well as some other groups,[27,28] and the Mo/S ratio of atmosphere in growth chamber was found decisive for the flake shapes in products.[29,30]

By contrast, the off-equilibrium or kinetic growth for crystals, which can yield dendrites,[31,32] precipitates,[33] epitaxial,[34] catalytic growth,[35] etc., is often associated with the supercooling, mass transport, strain or other environmental conditions. In

particular, the kinetic growth of 1D nanowires has the well-known catalytic modes: vapor-liquid-solid (VLS)[36-38] or vapor-solid-solid (VSS),[39-40] so the nano-particle catalysts are attached to the active growth sites at the top/bottom/end of nanowires and render the 1D directional growth. In analogous, for 2D materials like 2D MoS_2, the VLS catalytic growth still works and has been recently reported to guide the growth of 2D MoS_2 nanoribbon.[36] However, the roles played by the catalytic particles are still not fully understood.

Owning to the higher thermodynamic energies, high-index facets can only be prepared by certain kinetic approaches in nanomaterials, via e.g. thermal effect,[41] surface tension (Rayleigh),[42] electrical current[43,44] induced surface instabilities. Herein, for the synthesis of 2D TMDs with high-index facets (edges), nanoparticle catalyst (KCl) was applied, together with the plasma pre-treatment on substrates, which can enhance the mass transport along the 2D flake edges and override the mass supply directly from the vapor phase. The enhanced mass transport on edges caused the surface instabilities on flake edges, viable for high-index faceting. The relationship between the catalyst particle sizes and the resulted faceting angles can be explained by the surface instability theory. Moreover, with this new growth method, regular hexagons were produced with robust control, which is challenging by other methods. Overall, our approach paves a new way to controllable engineering on the shapes and patterns for 2D TMD materials via direct growth.

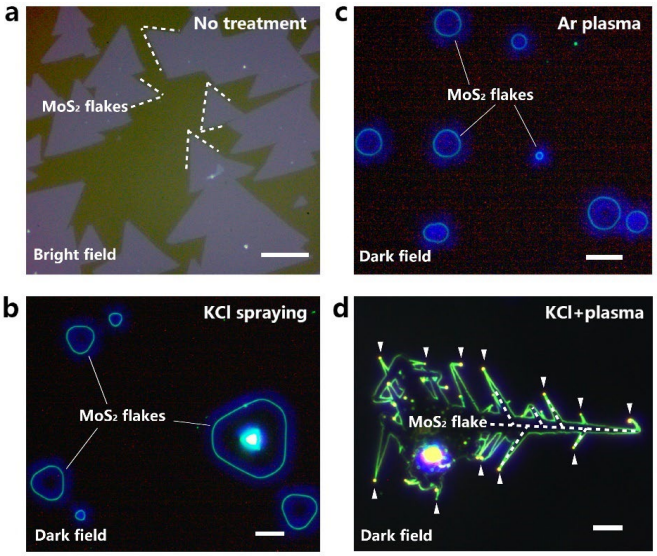

Figure 1. a) The bright field optical microscopy (OM) image of MoS_2 grown on no surface treatment sapphire substrate. Scale bar = 10 μm. b) The dark field OM images of MoS_2 grown on Ar plasma treated SiO_2/Si substrate. Scale bar = 5 μm. c) The dark field OM image of MoS_2 grown on KCl sprayed SiO_2/Si substrate. Scale bar = 5 μm. d) The dark field OM images of MoS_2 grown on Ar plasma treated combining with KCl sprayed fluorophlogopite mica substrate. The white arrows point out the catalytical particles. Scale bar = 10 μm.

RESULTS AND DISCUSSION

The 2D MoS_2 flake growth in our experiments was conducted by CVD[45] on sapphire, Si/SiO_2 and fluorophlogopite mica substrates, with special arrangements on the catalyst and pretreatments (see Figure S1 and Methods section in Supporting Information for details). The growth results with different conditions (for the KCl catalyst and Ar plasma pre-treatments) were compared. For the conventional CVD growth samples, with no KCl catalyst and Ar plasma treatment adopted, the conventional triangular/irregular monolayer MoS_2 flakes can be fabricated (Figure 1a, and results using different substrates shown in Supporting information, Figure S2). Meanwhile, if the KCl catalyst or Ar plasma treatments were treated separately, the typical growth results are presented in Figure 1b, c and supporting information Figure S2. These samples often had irregular shapes and non-straight edges, e.g. some had circle shapes, exhibiting the far-from-equilibrium growth manner. The growth kinetics overwhelmed the thermodynamic energies for the stable edges (facets) during growth.

Distinctly, the 2D MoS_2 samples grown with combined KCl catalyst and Ar plasma pre-treatment showed well-defined faceted edges, with catalyst particles on the corners (one on each corner) or sometimes on the edges (Figure 1d and supporting information Figure S2). More atomic force microscopy (AFM) and scanning electron microscopy (SEM) images, as well as Raman spectroscopy characterizations results on the flakes are presented in Figure S3-S10 in Supporting Information. The excellent crystallinity in the as-grown 2D MoS_2 flakes was clearly revealed, while most of the MoS_2 spikes/corners have the catalyst particles on top (end). The main composition of the catalytic particles were determined as K, Cl and Mo, S, Na and O according to the energy dispersive spectra (EDS) results (Supplementary Table S1). Considerable O and Na contents in the catalytical particles came from the vaporized precursor ($Na_2MoO_4 \cdot 2H_2O$) during growth, while molecular MoO_x and NaO_x were captured by the catalysts.

The growth of the acute angle 2D MoS_2 spikes were certainly driven by the leading catalyst particles on corners (Figure 2a). The invariable 120°/60° differences between the principle growth directions of the trunk and branches (white dashed lines in Figure 1d) showed the growth was still directed following the <100> crystal directions (zigzag directions) of MoS_2, however, a number of vicinal planes of {100} (viz. Mo or S zigzag planes) were present (Figure 2b) in the final products, which were different from the reported nanoribbon growth in parallel {100} planes (edges)[36]. {100} planes (edges) are the most stable edges of 2D MoS_2 according to previous reports.[46] However, the emerged high-index facets which could be identified by the acute angles of the spikes (white dashed lines in Figure 2a), were attributed to the growth kinetics.

Without KCl catalyst and plasma treatment, our CVD growth and supply of gaseous precursors in our growth chambers was lower than the threshold for kinetic growth. The surface instability on the low index edges, a signature for the kinetic growth, can be caused by the local inhomogeneity of mass transport. Owning to their strong ionic nature, the salts such as NaCl[47] and KCl can efficiently anchor the MoO_x and S species in the precursors and supply redox environment for growth radicals. In this way, the mass transport routes on the substrate surfaces or flake edges could be significantly altered by the enhanced deposition of precursors for MoS_2 growth. Besides, the Ar plasma treatment would clean the surface and possibly create surface dangling bonds on substrates (see supporting information Figure S11), enhancing the surface intimacy of substrates and the catalyst particles. Therefore, the edge diffusion assisted growth

led by cornered catalyst particles was triggered. A scheme of the catalyzed growth and associated mass transport is shown in Figure 2c. The atomic scale scanning transmission electron microscopy (STEM) results (Figure 2d) clearly show the distinct high-index vicinal edges produced by our kinetic growth approach. The atomic steps (highlighted by red triangles) are critical to control the adatom mobilities and edge instabilities.

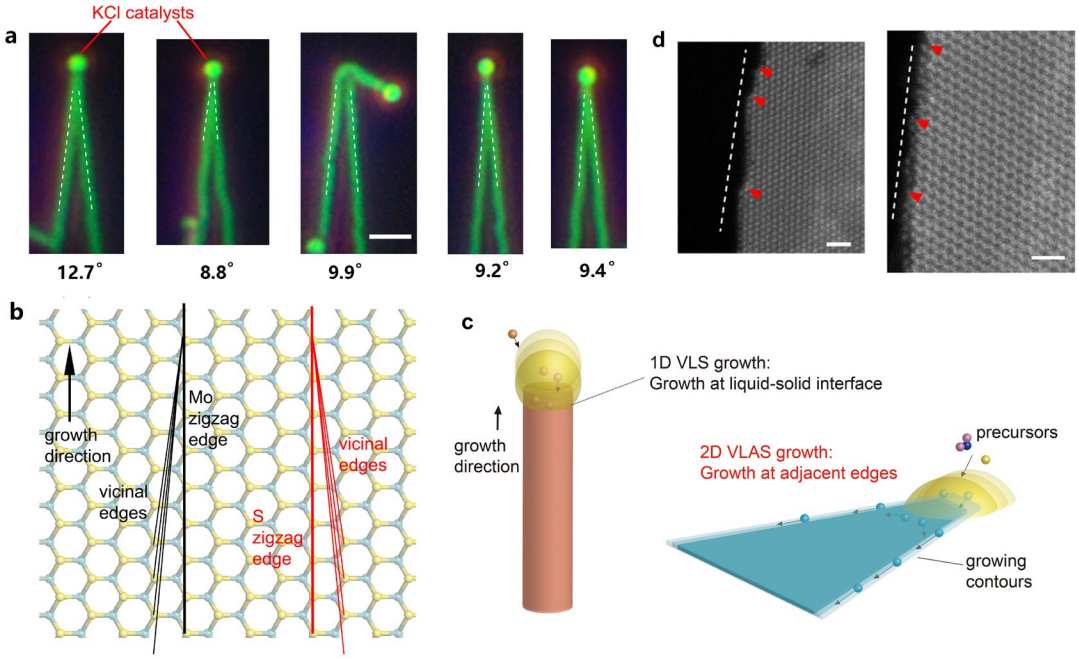

Figure 2. a) The magnified dark field images of MoS_2 branches in Figure 1d. Angles of each spike are shown below. Scale bar = 3 μm. b) The 2D MoS_2 atomic structure with vicinal planes of {100} (*viz.* Mo or S zigzag planes). The Mo atoms were blue and the S atoms were yellow. c) A schematic illustration of the catalyzed growth and associated mass transport. d) STEM-ADF images for the 2D MoS_2 (2L) flake edges grown by our kinetic approach. Atomic steps (marked by red triangles) are present in the high-index edges (white dash lines). Scale bars =1 nm.

The precursor overflow in catalyst particles and subsequent edge (surface) diffusion is apparently different in 2D materials growth from the 1D nanowire growth previously (Figure 2c). The interface of liquid/solid in 1D VLS growth can provide a sufficient area for absorption of oversaturated precursors, while in 2D growth case here, the oversaturated precursors are prone to be driven away from the underlying vdW surfaces to the more active edges. The directional rapid 1D edge diffusion is the key here as compared to the 2D surface diffusion for nanowire growth cases via this method. In has been found the cornered KCl catalysts and edge diffusion can also facilitate the growth of the exact regular hexagons of 2D MoS_2 (Figure 3a-c), implying the growth rate are independent on the thermodynamic differences between Mo and S-zigzag edges, the same as we observed in the vicinal edges for Mo and S-zigzag edges above. Figure 3a shows the optical images of the as-grown hexagonal flakes of 2D monolayer MoS_2. The KCl catalysts were present on all the corners and some edges. More interestingly, the atomic force microscopy (AFM) results (Figure 3c) indicated at all the corners of hexagons some additional faceted bulges induced by the edge instability were in presence. Unlike the perfect six-fold symmetrical shapes in these hexagons, the faceted small bulges were located at preferable edge types with only three-fold symmetry. At the same time, the growth without catalyst particles on corners mainly yielded regular triangle flakes under the same growth condition (Figure 3b).

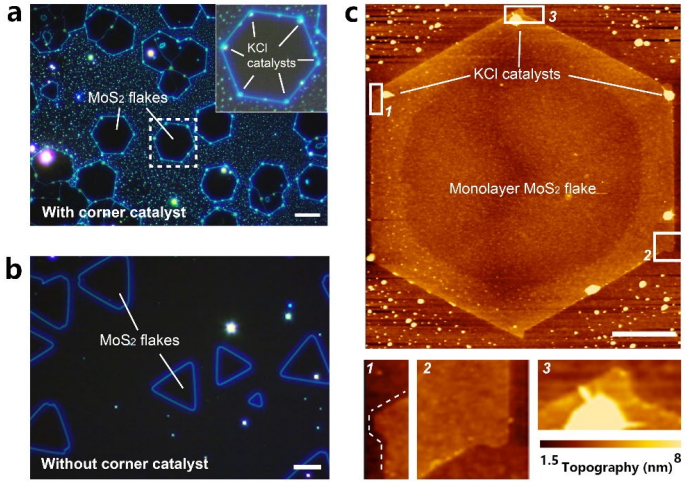

Figure 3. a) The dark field OM images of regular hexagonal monolayer 2D MoS_2 as grown on SiO_2/Si substrate with corner catalysts. The inset is magnified image for the dashed square zone. Scale bar=10 μm. b) The dark field OM image of triangle monolayer MoS_2 ¬as grown on substrate without corner catalyst. Scale bar=10 μm. c) The topographic atomic force microscopy (AFM) images of the hexagonal monolayer MoS_2 marked by the dashed square in Figure 3a. Numbered insets showed magnified images in white highlighted areas. Scale bar= 5 μm.

Since the conventional CVD growth of triangle flakes of 2D MoS_2 are predominantly observed and investigated by the atomistic growth simulations[48], the unusual perfect regular hexagon flakes of MoS_2 in our experiment are also attributed to the kinetic effect and explainable by the kinetic mass transport along edges. Manifested by the above growth products, in our CVD growth the catalyst particles not only served as the ordinary VLS catalyst that leads to direct growth at the local positions (point-like position) under the catalyst particles, instead, it promoted the growth nonlocally on the connected edges (Figure 2c). The non-equal Mo- and S-zigzag edges (or the opposite vicinal edges of Mo and S-zigzag edges) were grown at the same rate controlled/limited by the mass transport and precursor supply rate from the catalyst particles. A wealth of dangling bonds on edges provided the 1D diffusion channels. The atomic diffusion process was governing the mass transport on edges. Therefore, the growth mechanism here could be rationalized as vapor-liquid-adatom-solid (VLAS) process (Figure 4a), in comparison to the classical VLS mechanism. The mass (precursor) supply through the catalytic particles on corners/ends overwhelmed the direct gas phase supply, and the mass transport along edges became the growth rate limiting process for the entire kinetic growth.

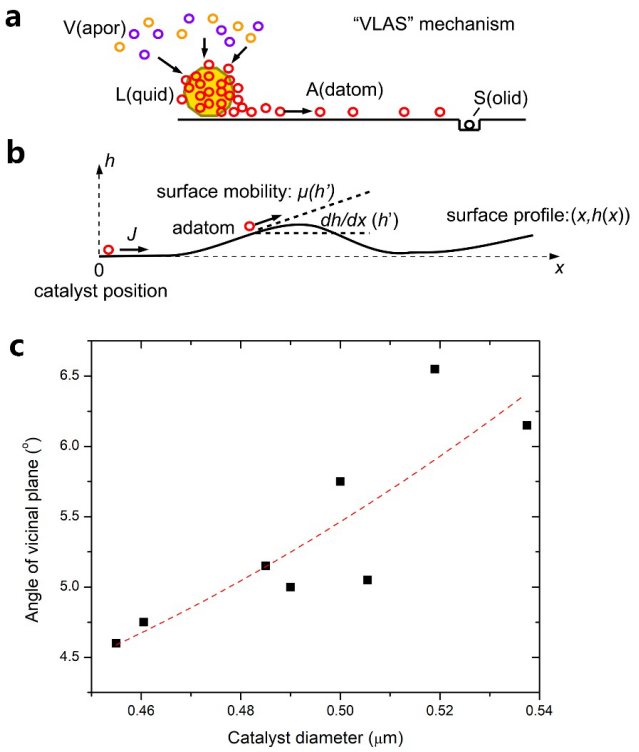

Figure 4. a) Schematic illustration of mechanism of VLAS growth. b) The surface instability induced by edge diffusion. c) The diagram of catalyst diameter dependence of angle of vicinal plane in the 2D MoS_2 samples, fitted by the instability model (red dashed line).

Here we use the surface instability model [49,50] usually for vicinal surface plane problems to explain the observed scenario of catalyst-led growth and the surface faceting. In view of the symmetric growth for Mo- and S-zigzag edges (or vicinal surfaces), the ratio of Mo/S of the source is not the governing factor, rather, the catalytic capture rate of precursors by KCl is critical. Thus the binary precursors for growth can be simply termed as adatom in the following. As depicted in Figure 4b, net flux of atoms(J) depends on a few variables, including local height (h), surface tension (σ), atom mobility (μ), and the adatom concentration (c), [49,50]

$$J(x) = \mu\sigma\cos\theta\frac{\partial^2(\sin\theta)}{\partial x^2} + \mu\frac{\partial c}{\partial x}, \qquad (1)$$

where x is the position, and $\sin\theta = \frac{\partial h}{\partial x}/\sqrt{1+(\frac{\partial h}{\partial x})^2}$. The first term on the right is the contribution from surface tension (inherent surface flattening), and the second term is contributed by the adatom diffusion along edges (the catalyst induced mass transport). μ is dependent on the slope (crystal plane of surface). For vicinal planes (edges for 2D flakes here), the mobility μ is inversely related to ∂h/∂x. The crystal growth rate h(t) is associated with J by dh/dt=∂J/∂x.

The above eq.(1) is a moving boundary problem. Considering the nature of the single source diffusion from the corners (catalyst), the adatom concentration gradient (∂c/∂x) gradually decreases from the corner points toward the center of the edges. For simplification, assuming a constant concentration gradient (K), surface instability wavelength (λ, the maximum straight length of edge) is given by,

$$\lambda \sim 2\pi\sqrt{\frac{\sigma}{\mu' K}} \qquad (2)$$

Therefore, the surface instability will be first initiated close to the catalyst location (*viz.*, at the corners with the largest K), then for the suppression of instability (keep the straightness of high-index vicinal surface), a minimum vicinal angle (α) is requested, yielding the straight vicinal edges near the corners (and catalytic particles). Our experimentally observed faceting relationship (α-r), where r is the radius of catalyst particle so proportional to $K^{1/2}$, which can be explained by the above eq.2 (Figure 4c). The bulges at the hexagon corners (Figure 3c) has the surface instability origin as well, caused by the edge instabilities first developed at the highest concentration gradient positions (corners). The preferential bulge occurrence at certain type of edges can be rationalized by the slight differences in atomic mobilities (μ) on the two types of edges (Mo and S zigzag edges). Thus, the creation of vicinal edges in our products is directly associated with the edge diffusion, higher index facets with lower diffusivity are preferred for keeping the straight edges under larger flux of mass flow along edges.

CONCLUSION

In summary, here we have introduced a new catalytic kinetic approach for the controllable synthesis of high-index edges as well as well-defined highly-symmetrical shapes of 2D TMD materials. This kinetic VLAS growth can overwhelm the thermodynamic factors which limit the product shapes. In such deep kinetic growth, the edge instability dependent on the mass transport along edges play a major role in controlling the final

edges. Overall, it is promising to achieve the well-controlled kinetic CVD growth of 2D materials by the introduction of catalytic particles and special pre-treatments on growth substrates. This new approach can significantly enrich the morphologies and patterns simply by growth method, and has potentials in electrical and electrochemical applications.

ASSOCIATED CONTENT

Supporting Information

The Supporting Information is available free of charge at

https://pubs.acs.org/doi/XXXXXXXX

Synthesis, crystallography, and characterization details

(PDF)

AUTHOR INFORMATION

Corresponding Author

* Jiong Zhao, jiongzhao@polyu.edu.hk

* Thuc Hue Ly, thuchly@cityu.edu.hk

ACKNOWLEDGMENT

This work was supported by National Science Foundation of China (Project No. 51872248, 51922113), Early Career Scheme CityU (Project No. 21303218), City University of Hong Kong (Project No. 9610387, 9680241, 7005259), the Hong Kong Research Grant Council under Early Career Scheme (Project No.25301018) and the Hong Kong Research Grant Council General Research Fund (Project No. 15302419). We thank Kin Wai Tong and Tianpeng Jiao for their help on experiment preparation.

REFERENCES

(1) Lopez-Sanchez, O.; Lembke, D.; Kayci, M.; Radenovic, A.; Kis, A. Ultrasensitive Photodetectors Based on Monolayer MoS_2. *Nat. Nanotechnol*. **2013,** 8, 497-501.

(2) Radisavljevic, B.; Radenovic, A.; Brivio, J.; Giacometti, V.; Kis, A. Single-Layer MoS_2 Transistors. *Nat. Nanotechnol*. **2011**, 6, 147-150.

(3) Ubrig, N.; Ponomarev, E.; Zultak, J.; Domaretskiy, D.; Zolyomi, V.; Terry, D.; Howarth, J.; Gutierrez-Lezama, I.; Zhukov, A.; Kudrynskyi, Z. R.; Kovalyuk, Z. D.; Patane, A.; Taniguchi, T.; Watanabe, K.; Gorbachev, R. V.; Fal'ko, V. I. Morpurgo A. F. Design of Van der Waals Interfaces for Broad-Spectrum Optoelectronics. *Nat. Mater*. **2020**, 19, 299-304.

(4) Wang, Q. H.; Kalantar-Zadeh, K.; Kis, A.; Coleman, J. N.; Strano, M. S. Electronics and Optoelectronics of Two-Dimensional Transition Metal Dichalcogenides. *Nat. Nanotechnol*. **2012**, 7, 699-712.

(5) Li, H. K.; Fong, K. Y.; Zhu, H. Y.; Li, Q. W.; Wang, S. Q.; Yang, S.; Wang, Y.; Zhang, X. Valley Optomechanics in a Monolayer Semiconductor. *Nat. Photonics*. **2019**, 13, 397-401.

(6) Mak, K. F.; Xiao, D.; Shan, J. Light-Valley Interactions in 2D Semiconductors. *Nat. Photonics.* **2018**, 12, 451-460.

(7) Hong, X. P.; Kim, J.; Shi, S. F.; Zhang, Y.; Jin, C. H.; Sun, Y. H.; Tongay, S.; Wu, J. Q.; Zhang, Y. F.; Wang, F. *Nat. Nanotechnol*. Ultrafast Charge Transfer in Atomically Thin MoS_2/WS_2 Heterostructures. **2014**, 9, 682-686.

(8) Okada, M.; Kutana, A.; Kureishi, Y.; Kobayashi, Y.; Saito, Y.; Saito, T.; Watanabe, K.; Taniguchi, T.; Gupta, S.; Miyata, Y.; Yakobson, B. I.; Shinohara, H.; Kitaura, R. Direct and Indirect Interlayer Excitons in a Van der Waals Heterostructure of $hBN/WS_2/MoS_2/hBN$. *ACS Nano* **2018**, 12, 2498-2505.

(9) Bediako, D. K.; Rezaee, M.; Yoo, H.; Larson, D. T.; Zhao, S. Y. F.; Taniguchi, T.; Watanabe, K.; Brower-Thomas, T. L.; Kaxiras, E.; Kim, P. Heterointerface Effects in the Electrointercalation of Van der Waals Heterostructures. *Nature* **2018**, 558, 425-429.

(10) Roy, T.; Tosun, M.; Hettick, M.; Ahn, G. H.; Hu, C. M.; Javey, A. 2D-2D Tunneling Field-Effect Transistors using $WSe_2/SnSe_2$ Heterostructures. *Appl. Phys. Lett*. **2016**, 108, 083111.

(11) Yu, Y. F.; Hu, S.; Su, L. Q.; Huang, L. J.; Liu, Y.; Jin, Z. H.; Purezky, A. A.; Geohegan, D. B.; Kim, K. W.; Zhang, Y.;

Cao, L. Y. Equally Efficient Interlayer Exciton Relaxation and Improved Absorption in Epitaxial and Nonepitaxial MoS_2/WS_2 Heterostructures. *Nano Lett*. **2015**, 15, 486-491.

(12) Chowdhury, T.; Kim, J.; Sadler, E. C.; Li, C. Y.; Lee, S. W.; Jo, K.; Xu, W. N.; Gracias, D. H.; Drichko, N. V.; Jariwala, D.; Brintlinger, T. H.; Mueller, T.; Park, H. G.; Kempa, T. J. Substrate-Directed Synthesis of MoS_2 Nanocrystals with Tunable Dimensionality and Optical Properties. *Nat. Nanotechnol.* **2020**, 15, 29-34.

(13) Cong, C. X.; Shang, J. Z.; Wu, X.; Cao, B. C.; Peimyoo, N.; Qiu, C.; Sun, L. T.; Yu, T. Synthesis and Optical Properties of Large-Area Single-Crystalline 2D Semiconductor WS_2 Monolayer from Chemical Vapor Deposition. *Adv. Opt. Mater.* **2014**, 2, 131-136.

(14) Lee, Y. H.; Zhang, X. Q.; Zhang, W. J.; Chang, M. T.; Lin, C. T.; Chang, K. D.; Yu, Y. C.; Wang, J. T. W.; Chang, C. S.; Li, L. J.; Lin, T. W. Synthesis of Large-Area MoS_2 Atomic Layers with Chemical Vapor Deposition. *Adv. Mater*. **2012**, 24, 2320-2325.

(15) Eichfeld, S. M.; Colon, V. O.; Nie, Y.; Cho, K.; Robinson, J. A. Controlling Nucleation of Monolayer WSe_2 during Metal-Organic Chemical Vapor Deposition Growth. *2D Mater.* **2016**, 3, 025015.

(16) Kim, H.; Ovchinnikov, D.; Deiana, D.; Unuchek, D.; Kis, A. Suppressing Nucleation in Metal-Organic Chemical Vapor Deposition of MoS_2 Monolayers by Alkali Metal Halides. *Nano Lett*. **2017**, 17, 5056-5063.

(17) Zhou, D.; Shu, H. B.; Hu, C. L.; Jiang, L.; Liang, P.; Chen, X. S. Unveiling the Growth Mechanism of MoS_2 with Chemical Vapor Deposition: from Two-Dimensional Planar Nucleation to Self-Seeding Nucleation. *Cryst. Growth. Des*. **2018**, 18, 1012-1019.

(18) Cong, C. X.; Shang, J. Z.; Wu, X.; Cao, B. C.; Peimyoo, N.; Qiu, C.; Sun, L. T.; Yu, T. Synthesis and Optical Properties

of Large-Area Single-Crystalline 2D Semiconductor WS_2 Monolayer from Chemical Vapor Deposition. *Adv. Opt. Mater*. **2014**, 2, 131-136.

(19) Chen, W.; Zhao, J.; Zhang, J.; Gu, L.; Yang, Z. Z.; Li, X. M.; Yu, H.; Zhu, X. T.; Yang, R.; Shi, D. X. Oxygen-Assisted Chemical Vapor Deposition Growth of Large Single-Crystal and High-Quality Monolayer MoS_2. *J. Am. Chem. Soc*. **2015**, 137, 15632-15635.

(20) Yang, P. F.; Zou, X. L.; Zhang, Z. P.; Hong, M.; Shi, J. P.; Chen, S. L.; Shu, J. P.; Zhao, L. Y.; Jiang, S. L.; Zhou, X. B.; Huan, Y. H.; Xie, C. Y.; Gao, P.; Chen, Q.; Zhang, Q.; Liu, Z. F.; Zhang, Y. F. Batch Production of 6-Inch Uniform Monolayer Molybdenum Misulfide Catalyzed by Sodium in Glass. *Nat. Commun*. **2018**, 9, 979.

(21) Ringe, E.; Van Duyne, R. P.; Marks, L. D. Wulff Construction for Alloy Nanoparticles. *Nano Lett*. **2011**, 11, 3399-3403.

(22) Ma, T.; Ren, W. C.; Zhang, X. Y.; Liu, Z. B.; Gao, Y.; Yin, L. C.; Ma, X. L.; Ding, F; Cheng, H. M. Edge-Controlled Growth and Kinetics of Single-Crystal Graphene Domains by Chemical Vapor Deposition. *PNAS*. **2013**, 110, 20386-20391.

(23) Wang, S. S.; Rong, Y. M.; Fan, Y.; Pacios, M.; Bhaskaran, H.; He, K.; Warner, J. H. Shape Evolution of Monolayer MoS_2 Crystals Grown by Chemical Vapor Deposition. *Chem. Mater*. **2014**, 26, 6371-6379.

(24) Schweiger, H.; Raybaud, P.; Kresse, G.; Toulhoat, H. Shape and Edge Sites Modifications of MoS_2 Catalytic Nanoparticles Induced by Working Conditions: A Theoretical Study. *J. Catal*. **2002**, 207, 76-87.

(25) Deng, Q. M.; Thi, Q. H.; Zhao, J.; Yun, S. J.; Kim, H.; Chen, G.; Ly, T. H. Impact of Polar Edge Terminations of the Transition Metal Dichalcogenide Monolayers during Vapor Growth. *J. Phys. Chem. C*. **2018**, 122, 3575-3581.

(26) Ly, T. H.; Perello, D. J.; Zhao, J.; Deng, Q. M.; Kim, H.; Han, G. H.; Chae, S. H.; Jeong, H. Y.; Lee, Y. H. Misorientation-Angle-Dependent Electrical Transport Across Molybdenum Disulfide Grain Boundaries. *Nat. Commun*. **2016**, 7, 10426.

(27) Chen, Q.; Li, H. S.; Xu, W. S.; Wang, S. S.; Sawada, H.; Allen, C. S.; Kirkland, A. I.; Grossman, J. C.; Warner, J. H. Atomically Flat Zigzag Edges in Monolayer MoS_2 by Thermal Annealing. *Nano Lett.* **2017**, 17, 5502-5507.

(28) Cui, P.; Choi, J. H.; Chen, W.; Zeng, J.; Shih, C. K.; Li, Z. Y.; Zhang, Z. Y. Contrasting Structural Reconstructions, Electronic Properties, and Magnetic Orderings along Different Edges of Zigzag Transition Metal Dichalcogenide Nanoribbons. *Nano Lett.* **2017**, 17, 1097-1101.

(29) Cao, D.; Shen, T.; Liang, P.; Chen, X.; Shu. H. Role of Chemical Potential in Flake Shape and Edge Properties of Monolayer MoS_2. *J. Phys. Chem. C*. **2015**, 119, 4294-4301.

(30) Wang, J. W.; Cai, X. B.; Shi, R.; Wu, Z. F.; Wang, W. J.; Long, G.; Tang, Y. J.; Cai, N. D.; Ouyang, W. K.; Geng, P.; Chandrashekar, B. N.; Amini, A.; Wang, N.; Cheng, C. Twin Defect Derived Growth of Atomically Thin MoS_2 Dendrites. *ACS Nano* **2018**, 12, 635-643.

(31) Zhang, Y.; Ji, Q.; Han, G. F.; Ju, J.; Shi, J.; Ma, D.; Sun, J.; Zhang, Y.; Li, M.; Lang, X. Y.; Zhang, Y.; Liu, Z. Dendritic, Transferable, Strictly Monolayer MoS_2 Flakes Synthesized on $SrTiO_3$ Single Crystals for Efficient Electrocatalytic Applications. *ACS Nano* **2014**, 8, 8617-8624.

(32) Zhang, Y.; Ji, Q. Q.; Wen, J. X.; Li, J.; Li, C.; Shi, J. P.; Zhou, X. B.; Shi, K. B.; Chen, H. J.; Li, Y. C.; Deng, S. Z.; Xu, N. S.; Liu, Z. F.; Zhang, Y. F. Monolayer MoS_2 Dendrites on a Symmetry-Disparate $SrTiO_3$ (001) Substrate: Formation Mechanism and Interface Interaction. *Adv. Funct. Mater*. **2016**, 26, 3299-3305.

(33) Wang, H. W.; Skeldon, P.; Thompson, G. E. XPS Studies of MoS_2 Formation from Ammonium Tetrathiomolybdate Solutions. *Surf. Coat. Tech*. **1997**, 91, 200-207.

(34) Wan, Y.; Xiao, J.; Li, J. Z.; Fang, X.; Zhang, K.; Fu, L.; Li, P.; Song, Z. G.; Zhang, H.; Wang, Y. L.; Zhao, M.; Lu, J.; Tang, N.; Ran, G. Z.; Zhang, X.; Ye, Y.; Dai, L. Epitaxial Single-Layer MoS_2 on GaN with Enhanced Valley Helicity. *Adv. Mater*. **2018**, 30, 1703888.

(35) Kim, H.; Han, G. H.; Yun, S. J.; Zhao, J.; Keum, D. H.; Jeong, H. Y.; Ly, T. H.; Jin, Y.; Park, J. H.; Moon, B. H. Role of Alkali Metal Promoter in Enhancing Lateral Growth of Monolayer Transition Metal Dichalcogenides. *Nanotechnology* **2017**, 28, 36LT01.

(36) Li, S. S.; Lin, Y. C.; Zhao, W.; Wu, J.; Wang, Z.; Hu, Z. H.; Shen, Y. D.; Tang, D. M.; Wang, J. Y.; Zhang, Q. Vapour-Liquid-Solid Growth of Monolayer MoS_2 Nanoribbons. *Nat. Mater*. **2018**, 17, 535-542.

(37) Li, S. Y.; Lin, P.; Lee, C. Y.; Tseng, T. Y. Field Emission and Photofluorescent Characteristics of Zinc Oxide Nanowires Synthesized by a Metal Catalyzed Vapor-Liquid-Solid Process. *J. Appl. Phys*. **2004**, 95, 3711-3716.

(38) Wagner, R. S.; Ellis, W. C. Vapor-Liquid-Solid Mechanism of Single Crystal Growth. *Appl. Phys. Lett*. **1964**, 4, 89-90.

(39) Wu, S. F.; Huang, C. M.; Aivazian, G.; Ross, J. S.; Cobden, D. H.; Xu, X. D. Vapor-Solid Growth of High Optical Quality MoS_2 Monolayers with Near-Unity Valley Polarization. *ACS Nano* **2013**, 7, 2768-2772.

(40) Kolasinski, K. W. Catalytic Growth of Nanowires: Vapor-Liquid-Solid, Vapor-Solid-Solid, Solution-Liquid-Solid and Solid-Liquid-Solid Growth. *Curr. Opin. Solid State Mater. Sci*. **2006**, 10, 182-191.

(41) Tian, N.; Zhou, Z. Y.; Yu, N. F.; Wang, L. Y.; Sun, S. G. Catalytic Growth of Nanowires: Vapor-Liquid-Solid, Vapor-Solid-Solid, Solution-Liquid-Solid and Solid-Liquid-Solid Growth. *J. Am. Chem. Soc*. **2010**, 132, 7580-7581.

(42) Lee, H. E.; Yang, K. D.; Yoon, S. M.; Ahn, H. Y.; Lee, Y. Y.; Chang, H.; Jeong, D. H.; Lee, Y. S.; Kim, M. Y.; Nam, K. T. Concave Rhombic Dodecahedral Au Nanocatalyst with Multiple High-Index Facets for CO_2 Reduction. *ACS Nano* **2015**, 9, 8384-8393.

(43) Zheng, S. J.; Carpenter, J. S.; Wang, J.; Mara, N. A.; Beyerlein, I. J. An Interface Facet Driven Rayleigh Instability in High-Aspect-Ratio Bimetallic Nanolayered Composites. *Appl. Phys. Lett*. **2014**, 105, 111901.

(44) Xiao, J.; Liu, S.; Tian, N.; Zhou, Z. Y.; Liu, H. X.; Xu, B. B.; Sun, S. G. Synthesis of Convex Hexoctahedral Pt Micro/Nanocrystals with High-Index Facets and Electrochemistry-Mediated Shape Evolution. *J. Am. Chem. Soc*. **2013**, 135, 18754-18757.

(45) Zhang, W. J.; Huang, J. K.; Chen, C. H.; Chang, Y. H.; Cheng, Y. J.; Li, L. J. High-Gain Phototransistors Based on a CVD MoS_2 Monolayer. *Adv. Mater*. **2013**, 25, 3456-3461.

(46) Li, Y. F.; Zhou, Z.; Zhang, S. B.; Chen, Z. F. MoS_2 Nanoribbons: High Stability and Unusual Electronic and Magnetic Properties. *J. Am. Chem. Soc*. **2008**, 130, 16739-16744.

(47) Kar, B. B.; Murthy, B. V. R.; Misra, V. N. Misra, Extraction of Molybdenum from Spent Catalyst by Salt-Roasting. *Int. J. Miner. Process* **2005**, 76, 143-147.

(48) Rajan, A. G.; Warner, J. H.; Blankschtein, D.; Strano, M. S. Generalized Mechanistic Model for the Chemical Vapor Deposition of 2D Transition Metal Dichalcogenide Monolayers. *ACS Nano* **2016**, 10, 4330-4344.

(49) Klug, J.; Dobbs, H. T. Current-Induced Faceting of Crystal Surfaces. *Phys. Rev. Lett*. **1994**, 73, 1947-1950;

(50) Zhao, J.; Yu, R.; Dai, S.; Zhu, J. Kinetical Faceting of the Low Index W Surfaces under Electrical Current. *Surf. Sci*. **2014**, 625, 10-15.

Table of Contents

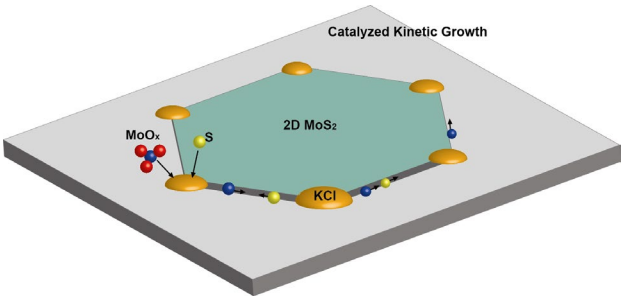

A catalyzed kinetic approach for unconventional morphology growth of two-dimensional transition metal dichalcogenides has been developed.